P-type semiconductor surfactant modified zinc oxide nanorods for hybrid bulk heterojunction solar cells

S. Ben Dkhil, M. Gaceur, W. Dachraoui, D. Hannani, S. Fall, F. Brunel, M. Wang, G. Poize, J. Mawyin, I. Shupyk, et al.

P-type semiconductor surfactant modified zinc oxide nanorods for hybrid bulk heterojunction solar cells

S. Ben Dkhil,[1] M. Gaceur,[1] W. Dachraoui,[1] D. Hannani,[1] S. Fall,[1] F. Brunel,[1] M. Wang,[1] G. Poize,[1] J. Mawyin,[1] I. Shupyk,[1] C. Martini,[1] E. Shilova,[1] F. Fages,[1] T. Ishwara,[2] J. Nelson,[2] T. Watanabe,[3] N. Yoshimoto,[3] O. Margeat,[1] C. Videlot-Ackermann,*[,1] and J. Ackermann*[,1]

[1]Aix-Marseille Université, CINaM CNRS, UMR 7325, 13288 Marseille, France

[2]Centre for Electronic Materials and Devices, Imperial College London, United Kingdom;

[3]Department of Materials Science and Engineering, Iwate University, Ueda Morioka 020-8551, Japan

[*] Corresponding Authors:
E-mail address: videlot@cinam.univ-mrs.fr (C. Videlot-Ackermann)
ackermann@cinam.univ-mrs.fr (J. Ackermann)

Abstract

In this work, hybrid bulk heterojunction solar cells based on surfactant-modified zinc oxide (ZnO) nanorods blended with poly-(3-hexylthiophene) (P3HT) are presented. (*E*)-2-cyano-3-(5'-(4-(dibutylamino)styryl)-2,2'-bithiophen-5-yl)acrylic acid (**1**), a p-type semiconductor, is used as grafted interfacial surfactant on ZnO nanorods in order to improve simultaneously the dispersion of ZnO nanorods inside the polymer blend as well as the electronic properties of the hybrid interface. The influence of surfactant concentration, solvent used for spin coating, and the P3HT:ZnO ratio on the nanoscale morphology of the P3HT/ZnO blends was studied by different techniques such as transmission electron microscopy (TEM), atomic force microscopy (AFM) and X-ray diffraction (XRD). The recombination dynamics of the photogenerated charges at the P3HT/ZnO interface were investigated by transient absorption spectroscopy (TAS) on micro- to millisecond time scales. For an optimal surfactant

concentration, it was found that the change of solvent (from to chloroform to orthodichlorobenzene) and an increased P3HT:ZnO ratio (from 1:0.5 to 1:2) yields four to six times of magnitude improvement in the nanocomposites photovoltaic cell efficiency. A solar power conversion efficiency of 0.93 % was achieved under AM1.5 illumination, corresponding to highly homogeneous dispersed ZnO nanorods in the P3HT polymer network. The improvement due to the ligand modification could be addressed to both improved electron transport in the nanocomposite films as well as increased interfacial area in combination with reproducible and controlled nanoscale morphology.

Keywords: ZnO nanorods; Ligands; P3HT; Surface modification; Hybrid materials; Solar cells; Nanoscale morphology.

1. Introduction

Hybrid photovoltaic cells based on a blend of inorganic nanocrystals and polymers are one of the promising low-cost, scalable solar power conversion using bulk heterojunctions and are interesting alternative to all organic solar cells. Such hybrid nanomaterials combine the electronic properties of inorganic materials with the low-temperature solution processability of polymers [1]. Different inorganic nanoparticles such as TiO_2 [2-4], ZnO [5-8], PbS [9, 10], CdS, CdSe or CdTe [11-14], and PbSSe [15] have been used as n-type semiconductor to produce hybrid bulk heterojunction solar cells with efficiencies up to 5.5%. Compared to all organic devices, these hybrid solar cells held great promises for aqueous solution processing and high temperature stability [16]. While high efficiencies could only obtained with nanoparticles bearing elements such as Cd or Pb, nontoxic alternatives based on metal oxide nanoparticles such as ZnO and TiO_2 show so far only poor efficiencies below 3% [17]. In order to improve device performances of metal oxide based hybrid solar cells,

interfacial modification of nanoparticles with ligands has been found very efficient [17]. For example, TiO_2 nanorods modified by dye molecules have been used as electron acceptor and demonstrated an improvement in the power conversion efficiency of solution processed P3HT/TiO_2 hybrid solar cells up to 2.2 % [18]. Improved charge carrier injection and passivation of trap states induced by the presence of surfactant at the TiO_2 surface were identified as key parameters. Such beneficial effect of ligand exchange was also demonstrated at the polymer/ZnO nanorod interfaces, for which ZnO nanorods were grown on ITO substrates and filled with P3HT to form a nanostructured hybrid solar cell or a planar structure between P3HT/ZnO [19, 20]. We previously demonstrated that porphyrin dye surfactants on the surface of ZnO nanorods contribute directly to the photocurrent generation in P3HT/ZnO blends and increase the spectral response of the solar cells. Unfortunately, we found that this dye, a tetra(4-caboxyphen)porphyrin, increases simultaneously the aggregation between nanorods due to strong dye-dye interaction leading finally to strong losses in all photovoltaic parameters of the devices [21]. Intensive studies were devoted to methods for improving the morphology of hybrid polymer blends by tailoring the compatibility of the nanoparticles with the polymer via ligand modification of the nanoparticles [13, 22-27]. These experiments reveal that in polymer/nanoparticle blends the surfactant controls not only the polymer-nanoparticle and the nanoparticle-nanoparticle interfaces, respectively, but also the nanoscale morphology of the blend that makes their choice critical for optimizing hybrid polymer blend solar cells. We could show recently that p-type bithiophene derivative monolayers grafted onto ZnO nanorods form a coaxial p-n junction core-shell systems that can be used instead of the polymer making the nanoscale control of the bulk heterojunction simpler [21, 28].

All these recent results of metal oxide based hybrid bulk heterojunctions point towards the crucial role of the interfacial modification of the inorganic surface via organic ligands to reach high efficiency. Taking into account the complex interplay between ligand, metal oxide and nanoscale morphology of the polymer blend, more fundamental work is needed to obtain a

deeper understanding of the different mechanisms involved in the device performance improvements. With this objective, we recently studied hybrid bilayer P3HT/ZnO solar cells with intercalated organic dyes at the hybrid interface [29]. It was shown that there is strong dye-ZnO and dye-P3HT interaction at the hybrid interface leading to changes in the open voltage of the solar cells. Furthermore, the dye can also reduce charge carrier recombination at the hybrid interface. As these experiments were performed with bilayer structure of very low efficiency, it would be very wishful for bulk heterojunction solar cells to use a suitable dye ligand that allow to increase the performance of the solar cells by increasing polymer-nanoparticle compatibility, with additional photocurrent generation properties and suitable energy level for reducing recombination kinetics at the hybrid interface.

In this work, we report on ZnO nanorods modified with a p-type semiconductor ligand bithiophene derivative, the (*E*)-2-cyano-3-(5'-(4-(dibutylamino)styryl)-2,2'-bithiophen-5-yl)acrylic acid (named **1**) [30], that allows a simple and versatile method to increase the dispersion of ZnO nanoparticles in P3HT polymer network and increase light absorption directly at the hybrid interface between ZnO and P3HT. From the molecular structure of **1** given in Figure 1, it can be seen that dibutyl group functionalizations are used to increase solubility of the nanorods via grafting that is obtained through the carboxylic acid group of **1.** The use of the acceptor cyano (-CN) group allows further to modify the band gap and thus to tune the energy position of the lower unoccupied energy level (LUMO) and the highest occupied energy level (HOMO) of the molecule in order to reduce the band gap and allow to absorb strongly in the visible [30]. A complete set of experiments is presented to elucidate the direct impact of solvent, P3HT:ZnO ratio and amount of molecules **1** grafted on ZnO on the nanoscale morphology, charge transport and the photocurrent generation properties of P3HT/ZnO blends.

2. Experimental part

Materials and device manufacture: Details on the synthesis of ZnO nanorods (NRs) and (E)-2-cyano-3-(5'-(4-(dibutylamino)styryl)-2,2'-bithiophen-5-yl)acrylic acid (**1**) are given elsewhere [30]. The as-produced ZnO single crystals have very smooth facets and a relatively well-controlled size distribution centered around 8 nm in diameter and 55 nm in length, as determined by high-resolution transmission electron microscopy (HR-TEM) (Figure 1a). The molecular structure of the low band gap oligomer **1** is given in Figure 1b. The HOMO and the LUMO levels of **1** were found to be 4.9 and 2.7 eV, respectively [30]. The molecule **1** was chosen as electroactive surfactant because of its good solubility in most organic solvent. Regioregular P3HT was purchased from Sigma-Aldrich (RR ≥ 90%). The synthesis of the modified **1**-ZnO NRs is particularly simple. Adding **1** to a solution of ZnO NRs produced hybrid nanostructures that can easily be isolated by centrifugation. To obtain the modified ZnO NRs, before mixing with P3HT solution, four different weights of **1** (0.5 wt%, 1 wt%, 2 wt% and 5 wt%) were added into the ZnO nanorod solutions. The carboxyl group of **1** graft to the surface of ZnO spontaneously and increase the solubility of ZnO NRs in the solution as can be seen in Figure 1c by the reduction of light scattering. In order to further reduce the amount of aggregates, the mixed solution was sonicated at 60°C for 20 min before spin coating, Modified **1**-ZnO NRs were mixed with P3HT in chloroform ($CHCl_3$), chlorobenzene (CB) or orthodichlorobenzene (ODCB) with different P3HT:ZnO ratios (1:0.5, 1:1 or 1:2). In order to make comparison, P3HT/ZnO films without adding **1** were also prepared. For each ratio, the P3HT concentration was kept constant at 15 mg/mL.

Solar cell fabrication: The devices were prepared on top of ITO glass substrate with a sheet resistivity of 15 Ω/square (Lumtec). A thin layer (40 nm) of PEDOT-PSS (poly(ethylenedioxythiophene)-poly(styrenesulfonate)) (CLEVIOS^{TM} AI 4083) was spin coated (4000 rpm for 60 s) in clean-room on top of the ITO to serve as a hole-only transport layer while also aiding to smooth out the ITO surface. The PEDOT-PSS layer was

subsequently annealed at 140°C during 20 min. The substrates were transferred in the glove-box for the deposition of the active layer. P3HT/**1**-ZnO composite films were prepared by spin-coating (1500 rpm for 60 s) the solution on top of the PEDOT-PSS layer without further annealing. For the final step, the substrates were then transferred outside of the glove-box for the electrodes deposition through evaporation of aluminum Al (120 nm) under vacuum. The device structure is given in Figure 1d.

Characterization and Testing: UV-vis absorption and fluorescence investigations of the P3HT/**1**-ZnO blend in thin films and its compounds in solution were recorded using a Varian 5000 UV-Vis-NIR spectrometer and a CARY Eclipse spectrometer, respectively. Morphological study of ZnO NRs were carried out by the high-resolution transmission electron microscope (HRTEM) JEOL 3010 (operating at an acceleration voltage of 300 kV), where samples are prepared by drop casting of diluted solution on a meshcoated carbon film. The TEM images of the P3HT/**1**-ZnO films were obtained by using the JEOL-3010 microscope with an accelerating voltage of 120 kV. Atomic force microscopy (AFM), by using a Nanoscope IIIA tapping mode multimode digital instrument, was used to characterize the roughness of P3HT/**1**-ZnO films. Furthermore, thin films were analyzed by two dimensional grazing incidence X-ray diffractometry (2D-GIXD) using high-brightness synchrotron radiation at BL19B2 in SPring-8. 2D-GIXD measurements were performed using high-sensitive 2D X-ray detector (PILATUS 300K) equipped with soller slit. The used incident angle and wavelength of X-ray in the experiments were 0.13° and 0.100 nm, respectively. The current density-voltage (J-V) characteristics were measured using a Keithley 238 Source Measure Unit inside the glove-box. Solar cell performance was measured by using a Newport class AAA 1.5 Global solar simulator (Oriel Sol3ATM model n°94043A) with an irradiation intensity of 100 mW/cm^2. In order to make comparison, P3HT/ZnO films without adding **1** were also prepared.

Field-effect transistor (FET) fabrication and characterization: Bottom-gate bottom-contact (BGBC) configuration was used for FET devices. The schematic representation of the FET architecture is shown in Figure S7. Interdigitated source and drain electrodes structured by a lift-off technique were deposited on n-doped silicon wafers covered with thermally grown silicon dioxide (SiO_2). Interdigitated electrodes were formed by 30 nm of gold (Au) and 10 nm of an adhesion layer of indium tin oxide (ITO). Such interdigitated FET structures were purchased from Fraunhofer (Germany) with a channel width W of 10 mm and different channel lengths L ranging from 2.5, 5, 10 and 20 μm. The capacitance per unit area of 230 nm thick SiO_2 dielectric layers was 14.6×10^{-9} F/cm^2. Prior the deposition of P3HT/**1**-ZnO films, the substrate was consecutively cleaned by ultra-sonication with acetone, isopropyl alcohol and rinsed with deionized water. The SiO_2 substrate was then dried and treated with final UV-ozone plasma for 5 min. The silicon oxide surface was modified with hexamethyldisilazane (HMDS) by spin-coating a solution in a two steps process (first step: 500 rpm for 5 s, second step: 4000 rpm for 40 s) and annealed at 135°C for 10 minutes in the glove-box. Spin-coating of the P3HT/**1**-ZnO active layer was performed then in the glove-box at 1200 rpm for 60 s following by a second step at 2000 rpm for 120 s. The samples were then left overnight under vacuum to remove residual solvent traces. Current-voltage characteristics were obtained with a Hewlett–Packard 4140B pico-amperemeter-DC voltage source. The mobilities were extracted from the saturation region of the transfer curves with the equation:

$$I_d = (W/2L)\, C_i \mu\, (V_g - V_t)^2 \qquad (1)$$

where I_d is the drain-source voltage, C_i is the capacitance per unit area of the gate insulator layer, V_g is the gate voltage, V_t is the threshold voltage, and μ is the field-effect mobility. Both FET fabrication and characterizations were performed in the nitrogen-filled glove box.

Transient absorption spectroscopy (TAS): The charge transfer properties of the P3HT/**1**-ZnO and P3HT/ZnO films were investigated through microsecond-millisecond TAS using an experimental configuration described elsewhere [13]. For this system, the excitation

(nitrogen-pumped dye laser, repetition rate ~4 Hz, pulse duration < 1 ns) was set to 520 nm, with a pump energy density of 45 $mJ.cm^{-2}.pulse^{-1}$. The transient absorption spectra were monitored by changing the probe wavelength (tungsten lamp) between 625 to 1050 nm.

3. Results and discussions

The p-type semiconducting ligand **1** was first grafted onto ZnO nanorods as interfacial surfactant. Figure 1b shows the molecular structure of **1** as well as a simplified energy diagram of this hybrid solar cell taking into account the energy level of molecule **1** and ZnO [21, 30]. It is worth mentioning that ZnO and P3HT as well as **1** form a type II heterojunctions. The large band offset between the LUMO level of **1** and the conduction band of the ZnO represents a strong driving force for exciton dissociation at the hybrid interface making photocurrent generation via the dye absorption possible [30]. Light absorption in P3HT should only lead to dissociation of excitons at the direct contact with the ZnO interface as there is energy off set of 0.3 eV between the LUMO of P3HT and **1**, respectively, hindering cascade reaction from P3HT to **1**. Thus we can expect that there is a competition in photocurrent generation at the hybrid interface between P3HT and **1**. By varying the amount of **1** at the ZnO surface, contribution of the ligand is expected to increase.

Grafting of **1** onto the ZnO NRs is first visualized by optical changes of the solution. Prior to grafting, ZnO NRs form aggregates in solution as indicated by strong light scattering of the solution (Figure 1c). Once a small amount (2 wt%) of **1** is grafted, the solubility of the nanorods bearing such interfacial surfactant increased dramatically so that stable solutions of **1**-ZnO can be obtained in ODCB. The formation of **1**-ZnO was further investigated by absorption spectroscopy. Figure 2a compares the absorption spectra of molecule **1**, ZnO NRs and **1**-ZnO in CB solution. The absorption maximum of compound **1** is located at λ_{max} = 498 nm while ZnO NRs have an absorption maximum around 360 nm. The measured spectrum of

1-ZnO corresponds principally to the combined molecule and ZnO absorption peaks. However the grafted molecules show a broader absorption band with a hypsochromic shift of 37 nm compared to **1** in solution. The blue-shift of the lowest-energy transition band (λ_{max} = 461 nm) in the hybrid nanostructure relative to the free ligand **1** (λ_{max} = 498 nm) correlate to our previous spectral observation made for a distyrylbithiophene derivative bearing a carboxylic acid function as ligand unit to bind the ZnO surface [28]. Such shift, first observed in thin films, was assigned to a crystalline organization of the parent nonsubstituted distyrylbithiophene via π-π stacking between the molecules [31-33]. Here we interpret the blue-shift as indicator that ligands **1** form aggregates on the ZnO surface in which the ligands organize perpendicular to the surface with the carboxylic group pointing to the surface of ZnO. Figure 2b shows the UV-Vis absorption spectra of bare P3HT/ZnO and modified P3HT/**1**-ZnO blends. Whereas P3HT and **1** has a strong absorption in the visible between 400 to 650 nm, the spectra of both P3HT/ZnO and P3HT/**1**-ZnO blends consist of the overlapping absorption bands of P3HT, **1** and ZnO. When increasing the amount of **1** at the surface of ZnO, we observe no apparent absorption characteristic to **1** for low concentration below 5%. In the case of higher concentration (10%), we find characteristic increase in light scattering indicating formation of large ZnO aggregates inside the polymer blend. Furthermore the two low-energy peaks at 550 and 600 nm of P3HT were used as indicator for highly crystalline P3HT phases [34-37]. It can be seen that bare P3HT/ZnO and modified P3HT/**1**-ZnO blends have almost absorption spectra with identical peak ratios. It is worth to noting that the same behavior is observed for P3HT/**1**-ZnO blends in chlorobenzene and chloroform solutions (Figure S1). Therefore, the photovoltaic properties of P3HT including exciton and hole transport should not be altered either by the presence of molecule **1** at the ZnO surface nor by the solvent.

Figure 2c shows the photoluminescence (PL) of bare P3HT/ZnO and modified P3HT/**1**-ZnO blends in comparison with P3HT. Whereas P3HT has the more intense PL

emission, both P3HT/ZnO and P3HT/**1**-ZnO blends induce a lower emission. The PL quenching of P3HT when mixed with ZnO NRs can be an indicator of the efficiency in exciton dissociation and charge transfer between P3HT and ZnO in the blends. The PL peak intensity of P3HT decreases by more than 10% in P3HT/ZnO blend and by 40% when **1** is added to the P3HT/ZnO blends as compared to pure P3HT indicating an improved generation of free charge carriers in the hybrid polymer blend.

Time resolved transient absorption spectroscopy (TAS) was used to study the photoinduced electron-transfer yield and charge recombination of the P3HT/ZnO nanorod interface upon grafting of **1**. TAS experiments were done on bare P3HT/ZnO blend samples, as reference, and modified P3HT/**1**-ZnO blend with 2 wt% of **1** for which optimal performances were obtained as described below. Figure 3 shows the transient absorption spectra of bulk heterojunction thin films at 10^{-6} s after excitation at 520 nm for bare P3HT/ZnO blend and modified P3HT/**1**-ZnO blend. For the reference sample, a wide absorption band appears with an absorption maximum at λ_{max} = 950 nm corresponding to the radical cation band of P3HT. In the case of P3HT/**1**-ZnO blend, an additional band with an absorption maximum at λ_{max} = 750 nm appears. This new band can be attributed to the radical cation band of **1** after charge carrier injection from the grafted molecules **1** to the ZnO NRs. This band was first observed for coaxial nanorod solar cells using **1** as light absorption and charge transporting layers in a previous publication [30]. The appearance of this **1**-assigned band clearly demonstrates that the surfactant not only influences the solubility of the ZnO nanorods, but also is involvend in the photogeneration process. The later can happen either via direct light absorption and followed by electron injection into ZnO. Alternatively, it could also arise from hole in injection from 1 to the radical cation state of P3HT by that improving photocurrent generation due to light absorption in the P3HT. By the fact that the amount of **1** concentration is very low, i.e. 2 wt%, the effect of additional photocurrent generation via absorption of the ligand is insignificant for photocurrent generation compared to P3HT.

Charge carrier recombination at the hybrid interface is therefore studied using excitation and probe wavelengths of 520 and 975 nm, respectively, for which P3HT radical absorption was a maximum. The TAS decay analysis in Figure 4 shows that the TAS intensity is strongly increased for modified **1**-ZnO NRs, which corresponds to the increase exciton quenching observed for these layers. Unmodified P3HT/**1**-ZnO blends show two components in the decay kinetics, one short and one long-lived decay. In contrast to our studies using porphyrin grafting at ZnO nanorods [21], for which the long-lived decay component was suppressed by the ligand and addressed to reduction of charge trapped at the hybrid interface, grafting of **1** is not affecting the intensity of the second long lived components. It is possible that rather direct interaction between the π-conjugated systems with the ZnO surface is involved in the passivation of trap state at the hybrid interface than the carboxylic acid groups used for the grafting of the ligand to the ZnO surface.

As a next step, we used transmission electron microscopy (TEM) and atomic force microscopy (AFM) to characterize the effect of **1** in the dispersion of ZnO in P3HT thin films. The morphology of spin-coated P3HT/**1**-ZnO blends is probed by TEM as shown in Figures 5 and S2 as function of grafted molecules on ZnO NRs (wt% from 0 to 5), P3HT:ZnO ratio (1:0.5, 1:1 and 1:2) and solvent ($CHCl_3$, ODCB and CB). The TEM images on Figure 5 clearly show that the dispersion of nanorods in the polymer is improved when the surfactant is added. Increasing the weight percentage wt% of **1** contributes to form homogeneous films by reducing the presence of ZnO aggregates (white circles in Figures 5). The ZnO NRs are randomly lying parallel to the surface plane. With 5 wt% of **1**, blending of **1**-ZnO and P3HT results in film bearing some ZnO free area of P3HT (black circles in Figures 5) indicating a beginning of phase separation between surface modificaed ZnO nanorods and P3HT. The origin of the ligand induced phase separation in not clear and deeper understand would go beyond this work, but we can conclude that best dispersion of ZnO NRs was found for 2% of **1**. We further compared to the dispersion of **1**-ZnO nanorods inside the polymer for the

optimal 2 wt% of **1** as a function of the solvent used and the mass ration of ZnO and P3HT. The TEM analysis of modified **1**-ZnO:P3HT films in Figure S2 show that solvent and mass ratio impact strongly the nanoscale morphology of the polymer ZnO blend. Best dispersion of NRs and thus best blend morphology were obtained with a P3HT:ZnO ratio of 1:2 in ODCB.

The blend morphologies observed with TEM were then compared with AFM analyze in tapping-mode (Figure 6 and S3). The film root mean square (rms) roughness of spin-coated P3HT/**1**-ZnO blends is summarized in Tables 1 and S1 as function of grafted molecules on ZnO NRs (wt% from 0 to 5) and solvent ($CHCl_3$, ODCB and CB). The AFM analysis clearly shows that bare P3HT/ZnO blend deposited by spin-coating contains large agglomerates in the films with a detrimental effect on the film roughness and thus potentially on device performance. After grafting of **1** on ZnO NRs with 0 to 5 wt%, the rms of modified P3HT/**1**-ZnO blends decreases from 13.02 to 8.66 nm, respectively, this can be assigned directly to the reduction of ZnO nanorod aggregates inside the polymer as seen as Figure 5. The effect of **1** grafting on morphological changes in P3HT/**1**-ZnO blends was further analyzed by XRD. From absorption spectroscopy, we showed crystalline organization of P3HT indicated by the two low energy peaks. The XRD analyze of pure P3HT layers reveal the presence of long range lamellar P3HT structure that lays parallel to the substrate surface (Figure S4). By adding either ZnO or **1**-ZnO NRs, a collapse of such lamellar structure of P3HT is observed together with the emergence of diffraction peaks corresponding to ZnO (Figure S5). Thus incorporation of ZnO nanorods, independently of their surface modification, suppresses long range organization inside the P3HT domains.

In order to study the photovoltaic properties of the polymer nanoparticle blends, hybrid solar cells were prepared via spin coating of P3HT/**1**-ZnO blends from solutions on indium tin oxide (ITO) covered glass substrates, which were coated with poly(3,4-ethylene-dioxythiophene)-poly(styrene-sulfonate) (PEDOT-PSS) before. Figure 1d illustrates a scheme of the corresponding device structure. All solar cells were characterized in an inert nitrogen

atmosphere (<0.1 ppm H_2O, < 0.1 ppm O_2) using a class AAA solar simulator. Figure 7 gives first the current density-voltage (J-V) curves of modified P3HT/**1**-ZnO blends as function of grafted molecules on ZnO NRs (wt% from 0 to 5) for a fixed P3HT:ZnO ratio of 1:2 in ODCB. We found that the addition of **1** to form modified **1**-ZnO NRs mixed with P3HT increases J_{sc}, V_{oc} and especially FF of the devices. Best performance was obtained for P3HT/**1**-ZnO blends with 2 wt% of grafted molecule. The device shows an open circuit voltage of V_{oc} = 0.72 V, a short-circuit current density J_{sc} = 1.94 mA/cm^2, and a fill factor of FF = 53% resulting in solar energy conversion efficiency of 0.93%. Compare to bare P3HT/ZnO blend, the solar energy conversion efficiency is increased from 0.14% to almost 1%. The low efficiency for unmodified ZnO is clearly correlated to the poor film morphology. Further increase in wt% of **1** to 5% lead to reduce photocurrent and FF. The reduction in photocurrent can be attributed to the worse nanoscale morphology compared to blends using 2 wt% of **1**, as observed in TEM analyses. Furthermore high amount of **1** at the surface of ZnO nanorods may generate exciton transfer barrier from P3HT to ZnO due to the LUMO off set of **1** compared to P3HT. The reduction in FF can be correlated to the formation of ZnO free areas observed at increasing concentrations of the surfactant (5 wt%) in TEM analysis. We further studied the impact of ZnO:P3HT ratio (1:0.5, 1:1 and 1:2) as well as solvent ($CHCl_3$, ODCB and CB) on the photovoltaic properties by using optimal 2% of **1** as shown in Figure S6. The corresponding photovoltaic parameters (open circuit voltage, V_{oc}; short-circuit current density, J_{sc}; fill factor, FF and power conversion efficiency, PCE) are summarized in Tables 1, S1 and S2. The analyses reveal the importance of the blend morphology, which was first studied by AFM and TEM for the performance of the device. Major impact in the photocurrent generation and fill factor is the aggregation free dispersion of **1**-ZnO NRs inside the P3HT. By the fact that **1** modified ZnO nanorods lead to poor device performance in $CHCL_3$ clearly shows that grafting of **1** only improves the device performance if a better dispersion of the ZnO nanorods is accompanied.

In order to get an insight into charge transport in the P3HT/**1**-ZnO composite structure, we performed FET measurements on thin films based on **1**-ZnO NRs mixed to P3HT polymer. Mixed solutions based on both **1**-ZnO NRs (2 wt%) and P3HT compounds were performed according to different P3HT/**1**-ZnO ratio (1:0.5, 1:1 and 1:2) in the three solvents (ODCB, CB and $CHCl_3$). Solutions were deposited by spin-coating onto Si/SiO_2 substrates equipped by Au interdigitated source and drain electrodes. The schematic representation of the FET architecture is shown in Figure S7. Current-voltage characteristics were performed in glove-box. Table 2 collects the electrical data in terms of hole and electron mobilities (μ) *vs.* P3HT/**1**-ZnO ratio and solvent. Purely p-channel FETs were realized for low P3HT:ZnO ratio with hole mobility up to $1\text{-}3\times10^{-3}$ $cm^2/V.s$. Such values are comparable to single P3HT based FETs with mobility of $2.4\text{-}2.6\times10^{-3}$ $cm^2/V.s$ [38]. When ZnO NRs are in excess to P3HT (ratio 1:2), an electron mobility is measured in ODCB and CB. The lack of electron transport in thin films based on $CHCl_3$ solution can be directly correlated to a reduce dispersion of nanorods in the polymer and the presence of large ZnO aggregates (see Figure S2). Electrons are confined in such unconnected aggregates without a percolation pathway through the entire bulk heterojunction. While both electron and hole transports are observed for ODCB and CB, more balanced mobilities are obtained for P3HT/**1**-ZnO blend as active layer processed from ODCB. Although still low electron transport, an ambipolar transport is measured (see Figure S8) with a hole mobility up to 1.7×10^{-4} $cm^2/V.s$ together with an electron mobility of 1×10^{-6} $cm^2/V.s$. Such observation highlights the great importance of an efficient and homogeneous dispersion of ZnO NRs in the polymer network for an electron transport and, more importantly, point also to one of the limitation of P3HT/**1**-ZnO blends in terms of obtaining efficient electron transport.

Our work aimed to optimize photocurrent generation properties of P3HT/ZnO blends based on ZnO NRs via use of p-type semiconductor ligands. However we found that incorporation of ligand modified ZnO NRs into P3HT leads to polymer blends with relatively

poor photocurrent generation efficiency although the nanorods are highly dispersed inside the P3HT. Indeed the ligand modification could improve the dispersion, nanoscale morphology including surface roughness and layer homogeneity of the blend, but only V_{oc} and FF were improved towards values that are comparable with polymer blends using fullerene acceptors. In contrast, the photocurrent is clearly lower than in all organic devices by approximately a factor 5. Possible reasons for this are the nanoscale morphology of the bulk heterojunction, charge carrier recombination inside the polymer blends as well as at the interfaces with the electrodes. From our photoluminescence analyses it was seen that the exciton quenching is not very efficient compared to blends using fullerene acceptors. In order to understand this residual lack of fluorescence quenching it is important to take into account the average distances between ZnO nanorods inside the polymer blends, which can be estimated to be less than 10 nm from our HR-TEM analysis on the corresponding thin films shown in Figure 5. Thus the residual excition quenching inside the polymer blend is difficult to be addressed to low dissociation efficiency of the hybrid interfaces. One reason for this may be the fact that the incorporation of ZnO NRs reduces strongly the long range crystalline organization of the P3HT as shown in Figure S4 and S5 making exciton diffusion towards to interface less efficient. By consequence, only a small amount of excitons reaches the hybrid interface leading to low photocurrent generation of the P3HT. Another strong limitation of the hybrid blends is the low electron mobility compared to the hole transport leading to unbalanced extraction of photogenerated charges and thus increased recombination inside the blend.

4. Conclusion

P-type semiconductor ligand modification of ZnO nanorods was studied to increase the photovoltaic performance of P3HT/ZnO devices. We could show that both ligand and P3HT can simultaneously generate photocurrent which is in accordance to our studies on porphyrin

and phthalocyanine molecules incorporated at hybrid P3HT:ZnO interface. But more importantly, we could demonstrate the importance of the ligand to the generation of ZnO aggregate free polymer/ZnO blend for high power conversion efficiency and corresponding photogenerated charge carrier transport. With the fine tuning of P3HT:ZnO ratio, choice of the solvent and an optimal surfactant concentration, both p- and n- charge carrier transport could be optimized inside the blend of P3HT/**1**-ZnO to form so-called ambipolar FETs together with a great effect on the photovoltaic parameters (V_{oc}, J_{sc}, FF and PCE). The best device, based on P3HT/**1**-ZnO blend as active layer spin-coated from a solution in ODCB at P3HT:ZnO ratio of 1:2 together with 2 wt% of **1** grafted on ZnO NRs, shows a J_{sc} of 1.94 mA /cm^2, V_{oc} of 0.72 V, FF of 53% and PCE of 0.93% respectively. While FF and V_{oc} were optimized to values comparable to P3HT blends using fullerene acceptors, photocurrent density was found low even after device optimization. This could be addressed to destruction of long rang organization of P3HT induced by the presence of the ZnO nanorods as well as low electron transport inside the blend. To further improve photocurrent generation in such hybrid polymer blends, development of suitable n-type ligands that improve both compatibility with the polymer as well as electron transport between ZnO nanorods may lead to raising power conversion efficiency of hybrid bulk heterojunctions solar cells to level of all organic devices.

Acknowledgements

S.B.D., M.G., W.D., D.H., S.F., F.B. and J.A. acknowledge financial support from the French FUI SFUMATO project (Grant number: F1110019V/201308815). M.W., G.P., J.M., I.S., C.M., E.S. and J.A. acknowledge financial support from OSEO and VALORPACA (Grant NANOHYBA). T.I. and J.N. acknowledge EPSRC for research Grants EP/G031088/1 and EP/E036341 and J. R. Durrant for discussions. The synchrotron radiation experiments were

performed by T.W. and N.Y. at BL19B2 in SPring-8 with the approval of Japan Synchrotron Radiation Research Institute (JASRI) (Proposal Nos. 2009B2070 and 2012 AB0036).

Supporting Information. Complementary figures on absorption spectra of P3HT/**1**-ZnO blends, TEM and AFM images of solar cell layers based on P3HT/**1**-ZnO blends, XRD analysis of P3HT/**1**-ZnO blends, I-V curves and photovoltaic parameters of P3HT/**1**-ZnO solar cells, and output characteristics of P3HT/**1**-ZnO films used as active layers in FETs.

References

[1] D.J. Milliron, I. Gur, A.P. Alivisatos, MRS .Bull., Hybrid Organic-nanocrystal solar cells, 30 (2005) 41-44.

[2] C.Y. Kwong, W.C.H. Choy, A.B. Djurisic, P.C. Chui, K.W. Cheng, W.K .Chan, Poly(3-hexylthiophene):TiO_2 nanocomposites for solar cell applications, Nanotechnology, 15 (2004) 1156-1161.

[3] P.A. van Hal, M.M. Wienk, J.M. Kroon, W.J.H. Verhees, L.H. Slooff, W.J.H. van Gennip, P. Jonkheijm, R.A.J. Janssen, Photoinduced electron transfer and photovoltaic response of a MDMO-PPV:TiO_2 bulk-heterojunction, Adv. Mater., 15 (2003) 118-121.

[4] C.Y. Kwong, A.B. Djurisic, P.C. Chui, K.W. Cheng , W.K. Chan, Influence of solvent on film morphology and device performance of poly(3-hexylthiophene):TiO_2 nanocomposite solar cells, Chem. Phys. Lett., 384 (2004) 372-375.

[5] W.J.E. Beek, M.M. Wienk, R.A.J. Janssen, Hybrid polymer solar cells based on zinc oxide, J .Mater .Chem., 15 (2005) 2985-2988.

[6] W.J.E. Beek, M.M. Wienk, R.A.J. Janssen, Efficient hybrid solar cells from zinc oxide nanoparticles and a conjugated polymer, Adv. Mater., 16 (2004) 1009-1013.

[7] W.J.E. Beek, L.H. Slooff, M.M. Wienk, R.A.J. Janssen, Adv. Func. Mater., Hybrid solar cells using a zinc oxide precursor and a conjugated polymer, 15 (2005) 1703-1707.

[8] W.J.E. Beek, M.M. Wienk, M. Kemerink, X.N. Yang, R.A.J. Janssen, Hybrid Zinc Oxide Conjugated Polymer Bulk Heterojunction Solar Cells, J. Phys. Chem. B, 109 (2005) 9505-9516.

[9] A.A.R. Watt, D. Blake, J.H. Warner, E.A Thomsen, E.L. Tavenner, H. Rubinsztein-Dunlop, P. Meredith, Lead sulfide nanocrystal: conducting polymer solar cells, J. Phys. D: Appl. Phys., 38 (2005) 2006-2012.

[10] J.H. Warner, A.A.R. Watt, Monodisperse PbS nanocrystals synthesized in a conducting polymer, Mater. Lett., 60 (2006) 2375-2378.

[11] W.U. Huynh, J.J. Dittmer, W.C. Libby, G.L. Whiting, A.P. Alivisatos, Adv. Funct. Mater., Controlling the morphology of nanocrystal–polymer composites for solar cells, 13 (2003) 73-79.

[12] B. Sun, E. Marx, N.C. Greenham, Photovoltaic devices using blends of branched CdSe nanoparticles and conjugated polymers, Nano Lett., 3 (2003) 961-963.

[13] B. Sun, H.J. Snaith, A.S. Dhoot, S. Westenhoff, N.C. Greenham, Vertically segregated hybrid blends for photovoltaic devices with improved efficiency, J. Appl. Phys., 97 (2005) 014914-5.

[14] J. Liu, T. Tanaka, K. Sivula, A.P. Alivisatos, J.M.J. Fréchet, Employing end-functional polythiophene to control the morphology of nanocrystal-polymer composites in hybrid solar cells, J. Am. Chem. Soc., 126 (2004) 6550-6551.

[15] Z. Liu, Y. Sun, J. Yuan, H. Wei, X. Huang, L. Han, W. Wang, H Wang, W Ma, High-efficiency hybrid solar cells based on polymer/PbS_xSe_{1-x} nanocrystals benefiting from vertical phase segregation, Adv. Mater. 2013, 25, 5772-5778.

[16] H. Wei, H. Zhang, G. Jin, T. Na, G. Zhang, X. Zhang, Y. Wang, H. Sun, W. Tian, B. Yang, Coordinatable and High Charge-Carrier-Mobility Water-Soluble Conjugated

Copolymers for Effective Aqueous-Processed Polymer–Nanocrystal Hybrid Solar Cells and OFET Applications, Adv. Funct. Mater. 2013, 23, 4035-4042.

[17] J. Bouclé, J. Ackermann, Solid-state dye-sensitized and bulk heterojunction solar cells using TiO2 and ZnO nanostructures: recent progress and new concepts at the borderline, Polymer International journal (In Focus), (2012), 61, 355-373.

[18] Y.-Y. Lin, T.-U. Chu, S.-S. Li, C.-H. Chuang, C.-H. Chang, W.-F. Su, C.-P. Chang, M.-W. Chu, C.-W. Chen, Interfacial nanostructuring on the performance of polymer/TiO_2 nanorod bulk heterojunction solar cells, J. Am. Chem. Soc., 131 (2009) 3644-3649.

[19] P. Ravirajan, A.M. Peiro, M.K. Nazeeruddin, M. Graetzel, D.C.D. Bradey, J.R. Durrant, J. Nelson, Hybrid polymer/zinc oxide photovoltaic devices with vertically oriented ZnO nanorods and an amphiphilic molecular interface layer, J. Phys. Chem. B, 110 (2006) 7635-7639.

[20] D.C. Olson, J. Piris, R.T. Collins, S.E. Shaheen, D.S. Ginley, Hybrid photovoltaic devices of polymer and ZnO nanofiber composites, Thin Solid Films, 496 (2006) 26-29.

[21] A.J. Said, G. Poize, C. Martini, D. Ferry, W. Marine, S. Giorgio, F. Fages, J. Hocq, J. Bouclé, J. Nelson, J.R. Durrant, J. Ackermann, Hybrid bulk heterojunction solar cells based on P3HT and porphyrin modified ZnO nanorods, J. Phys. Chem. C, 114 (2010) 11273-11278.

[22] I. Gur, N.A. Former, A.P. Alivisatos, Controlled assembly of hybrid bulk-heterojunction solar cells by sequential deposition, J. Phys. Chem. B, 110 (2006) 25543-25546.

[23] C.Y. Liu, Z.C. Holman, U.R. Kortshagen, Optimization of Si NC/P3HT hybrid solar cells, Adv. Funct. Mater., 20 (2010) 2157-2164.

[24] I. Gur, N.A. Fromer, C.-P. Chen, A.G. Kanaras, A.P. Alivisatos, Hybrid solar cells with prescribed nanoscale morphologies based on hyperbranched semiconductor nanocrystals, Nano Lett., 7 (2007) 409-414.

[25] K. Palaniappan, J.W. Murphy, N. Khanam, J. Horvath, H. Alshareef, M. Quevedo-Lopez, M.C. Biewer, S.Y. Park, M.J. Kim, B.E. Gnade, M.C. Stefan, Poly(3-hexylthiophene)-CdSe

quantum dot bulk heterojunction solar cells: influence of the functional end-group of the polymer, Macromolecules, 42 (2009) 3845-3848.

[26] H.J. Snaith, G.L. Whiting, B. Sun, N.C. Greenham, W.T.S. Huck, R.H. Friend, Self-organization of nanocrystals in polymer brushes. Application in heterojunction photovoltaic diodes, Nano Lett., 5 (2005) 1653-1657.

[27] N.C. Greenham, X. Peng, A.P. Alivisatos, Charge separation and transport in conjugated-polymer/semiconductor-nanocrystal composites studied by photoluminescence quenching and photoconductivity, Phys. Rev. B, 54 (1996) 17628-17637.

[28] C. Martini, G. Poize, D. Ferry, D. Kanehira, N. Yoshimoto, J. Ackermann, F. Fages, Oligothiophene Self-Assembly on the Surface of ZnO Nanorods: Toward Coaxial p-n Hybrid Heterojunctions, ChemPhysChem., 10 (2009) 2465-2470.

[29] G. Mattioli, S. Ben Dkhil, M.l. Saba, G. Malloci, C. Melis, P. Alippi, F. Filippone, P. Giannozzi, A.K. Thakur, M. Gaceur, O. Margeat, A.K. Diallo, C. Videlot-Ackermann, J. Ackermann, A.A. Bonapasta, A. Mattoni, Interfacial Engineering of P3HT/ZnO Hybrid Solar Cells Using Phthalocyanines: A Joint Theoretical and Experimental Investigation, Adv. Energ. Mat., (2014), 1301694-1301705.

[30] J. Mawyin, I. Shupyk, M. Wang, G. Poize, P. Atienzar, T. Ishwara, J.R. Durrant, J. Nelson, D. Kanehira, N. Yoshimoto, C. Martini, E. Shilova, P. Secondo, H. Brisset, F. Fages, J. Ackermann, Hybrid heterojunction nanorods for nanoscale controlled morphology in bulk heterojunction solar cells, J. Phys. Chem. C, 115 (2011) 10881-10888.

[31] C. Videlot-Ackermann, J. Ackermann, H. Brisset, K. Kawamura, N. Yoshimoto, P. Raynal, A. El Kassmi, F. Fages, α,ω-Distyryl-oligothiophenes: high mobility semiconductors for environmentally stable organic-thin film transistors, J. Am. Chem. Soc., 127 (2005) 16346-16347.

[32] C. Videlot-Ackermann, J. Ackermann, K. Kawamura, N. Yoshimoto, H. Brisset, P. Raynal, A. El Kassmi, F. Fages, Environmentally stable organic thin films transistors:

Terminal styryl *vs* central divinyl benzene building blocks for p-type oligothiophene semiconductors, Org. Electron., 7 (2006) 465-473.

[33] C. Videlot-Ackermann, H. Brisset, J. Zhang, J. Ackermann, S. Nénon, F. Fages, P. Marsal, T. Tanisawa, N. Yoshimoto, Influence of phenyl perfluorination on charge transport properties of distyryl-oligothiophenes in organic field-effect transistors, J. Phys. Chem. C, 113 (2009) 1567-1574.

[34] R. Zhang, B. Li, M.C. Iovu, M. Jeffries-El, G. Sauvé, J Cooper, S. Jia, S. Tristram-Nagle, D.M. Smilgies, D.N. Lambeth, R.D. McCullough, T. Kowalewski, Nanostructure Dependence of Field-Effect Mobility in Regioregular Poly(3-hexylthiophene) Thin Film Field Effect Transistors, J. Am. Chem. Soc., 128 (2006) 3480–3481.

[35] H. Sirringhaus, P.J. Brown, R.H. Friend, M.M. Nielsen, K. Bechgaard, B.M.W. Langeveld-Voss, A.J.H. Spiering, R.A.J. Janssen, E.W. Meijer, Microstructure-mobility correlation in self-organised, conjugated polymer field-effect transistors, Synth. Met., 111-112 (2000) 129-132.

[36] J.A. Merlo, C.D. Frisbie, Field effect transport and trapping in regioregular polythiophene nanofibers, J. Phys. Chem. B, 108 (2004) 19169-18179.

[37] J. M.Verilhac, G. LeBlevennec, D. Djurado, F. Rieutord, M. Chouiki, J.-P.Travers, A. Pron, Effect of macromolecular parameters and processing conditions on supramolecular organisation, morphology and electrical transport properties in thin layers of regioregular poly(3-hexylthiophene), Synth. Met., 156 (2006) 815-823.

[38] R.J. Kline, M.D. McGehee, E.N. Kadnikova, J. Liu, J.M.J. Fréchet, Adv. Mater., Controlling the field-effect mobility of regioregular polythiophene by changing the molecular weight, 15 (2003) 1519-1522.

Table 1: Photovoltaic parameters and thin film roughness of P3HT/**1**-ZnO composite films as function of grafted molecules **1** (wt%) (P3HT:ZnO ratio is 1:2 and solvent is ODCB).

wt% of **1**	rms (nm)	PCE (%)	V_{oc} (V)	J_{sc} (mA/cm^2)	FF (%)
0 %	13.02	0.14	0.37	0.92	33
0.5 %	11.71	0.33	0.59	1.19	38
1 %	9.99	0.71	0.68	1.72	49
2 %	9.69	0.93	0.72	1.94	53
5 %	8.66	0.69	0.71	1.66	46

Table 2: Electron (μ_e) and hole (μ_h) mobilities of P3HT/**1**-ZnO composite films as a function of P3HT:ZnO ratio and solvent.

ratio	solvent	μ_e (cm^2/V.s)	μ_h (cm^2/V.s)
1:0.5	ODCB	- [(1)]	1.7×10^{-3}
1:1	ODCB	- [(1)]	3.7×10^{-3}
1:2	ODCB	1×10^{-6}	1.7×10^{-4}
	CB	3×10^{-9}	1×10^{-3}
	$CHCl_3$	- [(1)]	3.2×10^{-4}

[(1)] Electron transport is not observed.

Figure captions

Figure 1: HR-TEM image of ZnO NRs (a), molecular structure of **1** and energy diagram of the bulk heterojunction solar cell using modified **1**-ZnO NRs and P3HT (b), optical image of orthodichlorobenzene solutions containing ZnO NRs (left) and modified **1**-ZnO nanorods with 2 wt% of **1** (right) (c), device structure based on the modified P3HT/**1**-ZnO blend (d).

Figure 2: (a) Absorption spectra of **1**, ZnO NRs and modified **1**-ZnO NRs (with 2 wt% of grafted molecules **1**) in CB solution. Absorption (b) and photoluminescence (c) spectra of P3HT polymer, P3HT/ZnO and P3HT/**1**-ZnO blends in ODCB solutions with P3HT:ZnO ratio of 1:2. Emission spectra were obtained upon excitation at 550 nm.

Figure 3: Transient absorption spectra at 10^{-6} s after excitation at 520 nm for P3HT/ZnO film (grey) and P3HT/**1**-ZnO film (black) from blends in ODCB with P3HT:ZnO ratio of 1:2. The P3HT/**1**-ZnO blend contain 2 wt% of grafted molecules **1**.

Figure 4: Transient absorption decays of P3HT/ZnO film (grey) and P3HT/**1**-ZnO film (black) from blends in ODCB with P3HT:ZnO ratio of 1:2. The P3HT/**1**-ZnO blend contain 2 wt% of grafted molecules **1**. (b) TAS decay normalized for simple as shown in part (a). Excitation and probe wavelength were at 520 and 975 nm, respectively.

Figure 5: TEM images of solar cell layers based on P3HT/**1**-ZnO blends in ODCB with P3HT:ZnO ratio of 1:2 as function of wt% of grafted molecules **1**. With 0 wt% of **1**, the blend corresponds to the reference P3HT/ZnO blend.

Figure 6: AFM images of solar cell layers based on P3HT/**1**-ZnO blends in ODCB with 2 wt% of grafted molecules **1** and a P3HT:ZnO ratio of 1:2.

Figure 7: J-V curves of solar cells based on P3HT/**1**-ZnO blends in ODCB as function of P3HT/ZnO ratio for 2 wt% of grafted molecules **1** (a) and as function of wt% of grafted molecules **1** for P3HT/ZnO ratio of 1:2 (b).

Figure 1

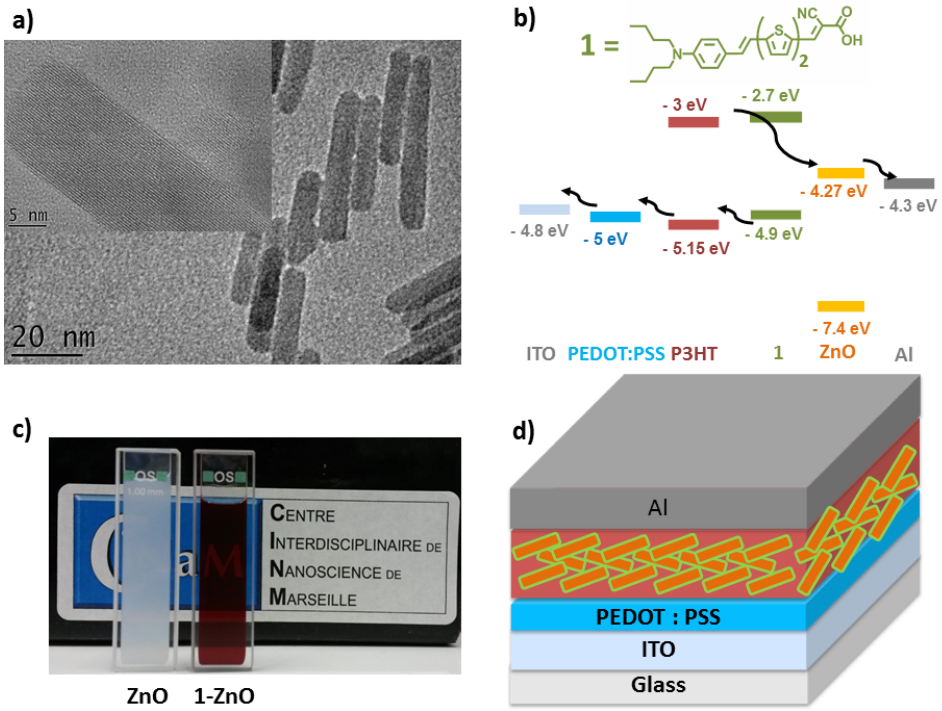
a)
5 nm
20 nm
b)
1 =
NC
O
OH
S
N
2
- 3 eV
- 2.7 eV
- 4.27 eV
- 4.3 eV
- 4.8 eV
- 5 eV
- 5.15 eV
- 4.9 eV
- 7.4 eV
ITO
PEDOT:PSS
P3HT
1
ZnO
Al
c)
CENTRE
INTERDISCIPLINAIRE DE
NANOSCIENCE DE
MARSEILLE
ZnO
1-ZnO
d)
Al
PEDOT : PSS
ITO
Glass

Figure 2

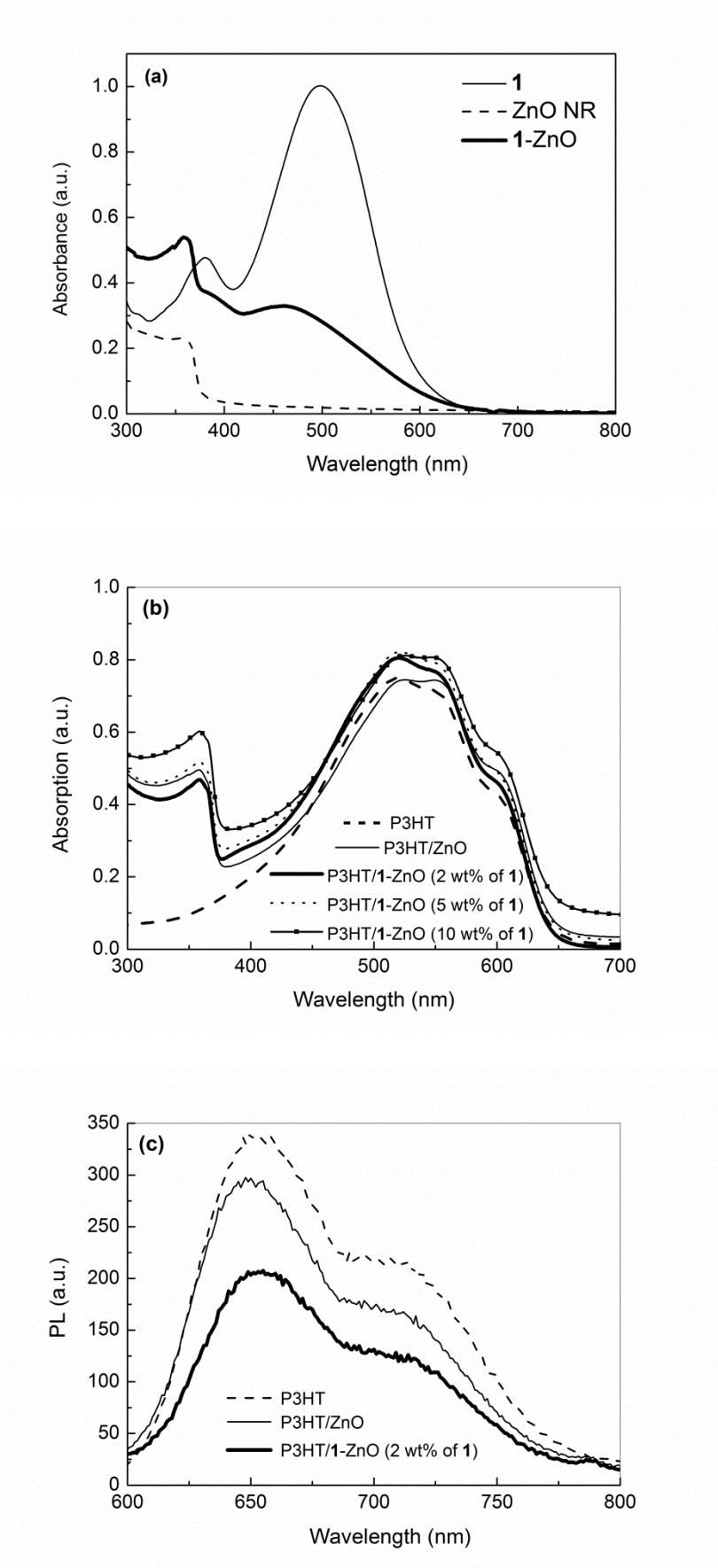
(a)
1
ZnO NR
1-ZnO
Absorbance (a.u.)
Wavelength (nm)
(b)
P3HT
P3HT/ZnO
P3HT/1-ZnO (2 wt% of 1)
P3HT/1-ZnO (5 wt% of 1)
P3HT/1-ZnO (10 wt% of 1)
Absorption (a.u.)
Wavelength (nm)
(c)
P3HT
P3HT/ZnO
P3HT/1-ZnO (2 wt% of 1)
PL (a.u.)
Wavelength (nm)

Figure 3

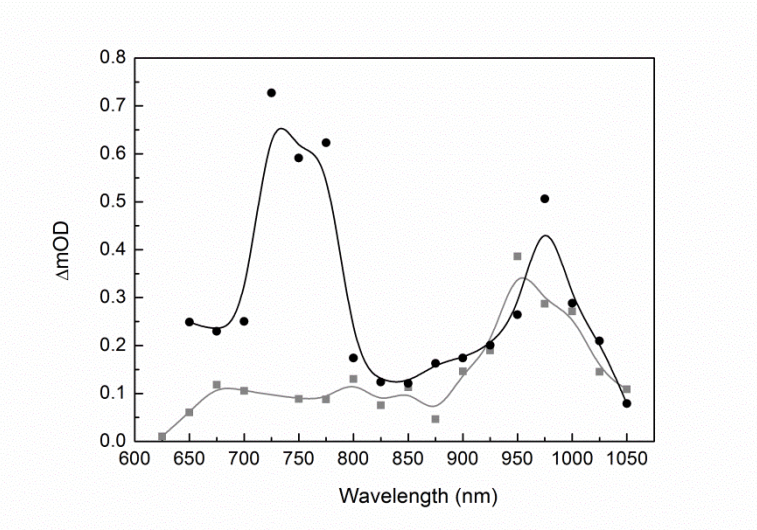

Figure 4

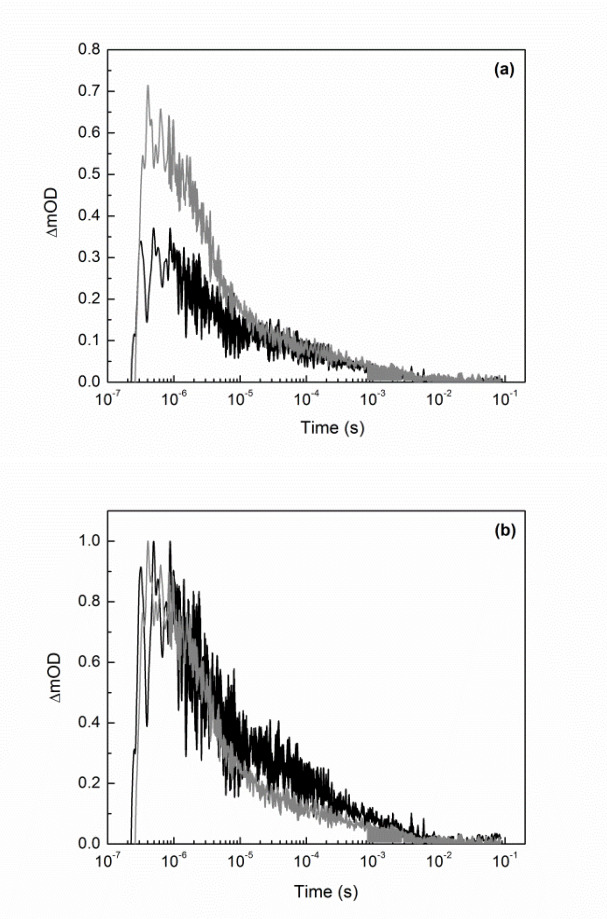

Figure 5

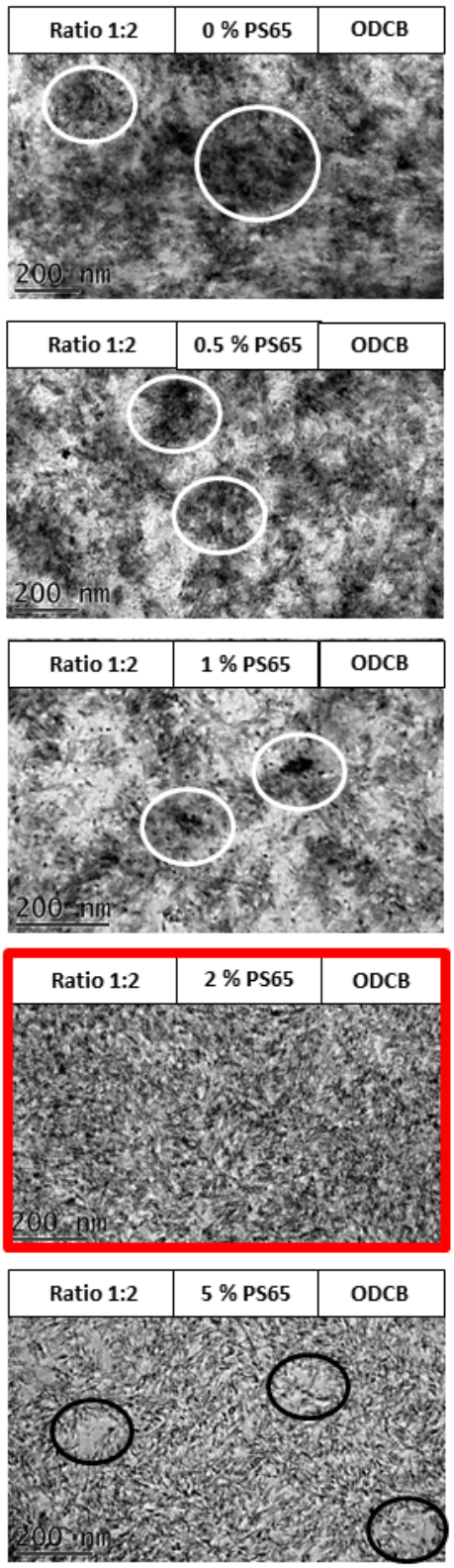
Ratio 1:2
0 % PS65
ODCB
200 nm
Ratio 1:2
0.5 % PS65
ODCB
200 nm
Ratio 1:2
1 % PS65
ODCB
200 nm
Ratio 1:2
2 % PS65
ODCB
200 nm
Ratio 1:2
5 % PS65
ODCB
200 nm

Figure 6

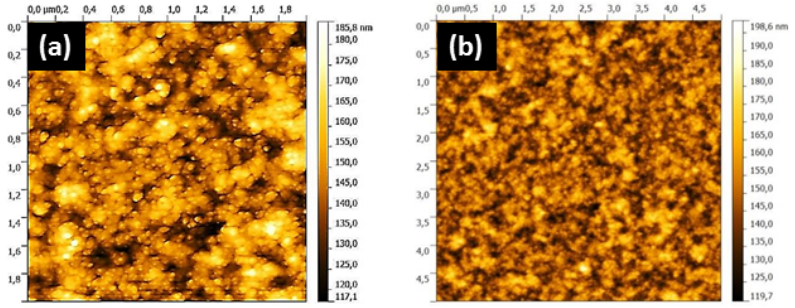

Figure 7